Barium and xenon isotope yields in photopion reactions of ^{133}Cs

K. Sakamoto, Y. Hamajima, M. Soto, Y. Kubota, M. Yoshida, A. Kunugise, and M. Masatani
Department of Chemistry, Faculty of Science, Kanazawa University, Kanazawa 920, Japan

S. Shibata and M. Imamura
Institute for Nuclear Study, University of Tokyo, Tanashi, Tokyo 188, Japan

M. Furukawa
Department of Chemistry, Faculty of Science, Nagoya University, Nagoya 464, Japan

I. Fujiwara
School of Economics, Otemon Gakuin University, Ibaragi, Osaka 567, Japan
(Received 6 October 1989)

Radiochemical yield measurements are reported for barium isotopes from ^{133}Cs$(\gamma,\pi^- xn)^{133-x}$Ba for $x=0$, 2, 4, 5, 6, 7, and 9 for bremsstrahlung maximum end-point energies $E_0=30$–1050 MeV and for ^{133}Xe from ^{133}Cs$(\gamma,\pi^+)^{133m,g}$Xe for $E_0=300$–1000 MeV. Emphasis was placed on Ba measurements near the pion threshold and for different target thicknesses in order to assess interfering secondary particle-induced reactions. Clear evidence of secondary reactions was found in the form of a shoulder in the yield curves for a range of values near $E_0 \lesssim Q_{\pi^-}$, the Q_{π^-} value of ^{133}Cs$(\gamma,\pi^- xn)$ reaction. This result was used for the correction of yields at $E_0 \gtrsim Q_{\pi^-}$ with the aid of reported measurements of photoproton spectra from ^{12}C and other complex nuclei and cross sections of (^{133}Cs$+p$) reactions. The yields corrected for the secondaries $\sigma_q(E_0)$ were unfolded into cross sections per photon of energy k, $\sigma(k)$. The characteristic features of $\sigma_q(E_0)$ and $\sigma(k)$ are then discussed in terms of E_0 and k dependences and product mass ($A_p=133-x$) by comparing the present results with those for other systems currently obtained by our group. It was found that the present results of $\sigma(k)$ are generally reproduced by a cascade-evaporation calculation based on the PICA code of Gabriel and Alsmiller, only if the calculated values are shifted up in photon energy by 30 MeV and the neutron cutoff energy is chosen to be 1 MeV.

I. INTRODUCTION

We report yield measurements for ^{133m,131m,g,129m,g,128,127,126,124}Ba from ^{133}Cs irradiated with a bremsstrahlung beam with maximum end-point energies of $E_0=30$ to 1050 MeV in steps of 50 MeV or less. The results for ^{133m,g}Xe at $E_0=300$, 500, 700, 800, 900, and 1000 MeV are also included. These radionuclides are expected to be produced from ^{133}Cs$(\gamma,\pi^- xn)$ and (γ,π^+) reactions. At energies above the pion threshold, the Δ isobar is expected to be produced by the resonance interaction of an incoming photon with a single nucleon N inside the target nucleus, whereas the nonresonant Born terms are responsible for the strong background for pion production, which varies with the energy. The isobar decays immediately (10^{-24} sec) into a stable nucleon and a pion, and both particles produced in these initial processes would usually develop a cascade-evaporation process in the same nucleus. During the process one or both of the particles may escape from the nucleus. The probability of the escape may depend on the location of photoabsorption by a nucleon and nuclear transparency for the associated particles. If the pion is emitted in forward direction at small angles, the nucleus would be left with an energy insufficient for developing the cascade-evaporation process. Especially, when photoabsorption occurs at the surface region of the target nucleus, the chance for an escape would be high and such simple reactions as (γ,n), (γ,p), and $(\gamma,\pi^\pm)$ could result. These simple reactions have received occasional attention in order to gain valuable information concerning photonuclear interactions and nuclear structure.[1–4] Additional emissions of nucleons, especially neutrons, will also occur if sufficient energy is left after the primary process. Neutron channels following pion emission have been studied far less extensively because of the experimental complexity regarding multiparticle coincidence. Otherwise, studies have been limited to inclusive experiments of low multiplicity.

Due to the absence of high-energy monochromatic photon sources with sufficiently high intensity, a bremsstrahlung beam of continuous spectrum characterized approximately by $1/k$ (k is the energy of constituent photons, ranging from zero up to the end-point energy E_0) has been a unique tool in photonuclear reaction studies. Exceptions are counter experiments in which tagged photons and annihilation radiations have been used. With bremmstrahlung, simple reactions are always accom-

panied by dominant reactions of single and multiple nucleon emissions, i.e., spallation, due to the giant resonance and quasideuteron mechanisms caused by low-energy photons up to $k = 100$ MeV, as well as that due to a cascade-evaporation process initiated by Δ decay. Among these simple reactions. (γ,π^+) and (γ,π^-,xn) reactions of $x \geq 0$ are easily distinguished from other processes by the use of radiochemical methods. Some measurements on (γ,π^+) on complex nuclei have been reported in the literature.[5-9] However, studies of the latter-type reactions have been reported only in very limited cases of ^{51}V $(\gamma,\pi^-)^{51}$Cr (Refs. 8 and 9), ^{51}V $(\gamma,\pi^-2n)^{49}$Cr (Refs. 5,7,9-13), and ^{51}V$(\gamma,\pi^-3n)^{48}$Cr (Refs. 9 and 13) and some others such as ^{197}Au$(\gamma,\pi^-xn)^{197-x}$Hg for $x = 0$, 2, 4, and 5 (Refs. 14-16). New clues to mechanism of photonuclear processes at intermediate energies are expected from a more thorough investigation of these photopion reactions.

A problem that plagues radiochemical methods is the presence of nonmesic interactions; secondary protons and neutrons lead to the same products of (γ,π^-xn) and (γ,π^+) reactions through $(p,x'n)$ and (n,p) reactions, respectively. The emphasis in the present work was placed on runs below and above thresholds for pion production and on runs on target stacks of different thickness in order to assess the contribution of interfering reactions. A successful correction for this contribution made it possible to characterize the new features of the cross section of the (γ,π^-xn) reaction on complex nuclei. A comparison of the present results in the form of $\sigma(k)$, cross section per photon of monochromatic energy k, as a function of k was made with a cascade-evaporation calculation based on Gabriel-Alsmiller's PICA code. This model has not been extensively tested with respect to $\sigma(k)$ since its publication in 1969.[17,18] Total photoabsorption cross sections are also considered.

II. EXPERIMENTAL

Three to four disks of CsCl, each about 0.35–0.5 g/cm^2 thick and 1 cm in diameter, were placed in a quartz tube together with Al, Ni, and/or Au beam monitors of thicknesses 6.9 (or 16.5), 13, and 100 mg/cm^2, respectively, on both sides of each disk. Irradiations were carried out in a water-cooled target holder for 5–10 min with an uncollimated bremsstrahlung beam of maximum endpoint energies 30 to 250 MeV from the 300-MeV Electron Linac of the Laboratory of Nuclear Science (LNS), Tohoku University.[19] A series of irradiation for $E_0 = 100$–250 MeV was performed with an electron beam being passed through an energy-compressing system;[20] the electron energy was confined to be $\pm 1\%$ at full width at half maximum (FWHM). Irradiation at $E_0 = 305$ MeV was performed in air with use of the 600-MeV Electron Linac at the Electrotechnical Laboratory (ETL) for a similar target system to the one at LNS. Both at LNS and ETL, bremsstrahlung was produced in a 0.5-mm-thick Pt converter and was not electron free. For $E_0 = 300$ to 1050 MeV irradiations were performed in 50-MeV steps for 30 min to 8 h in air with electron-free collimated bremsstrahlung from the 1.3-GeV Electron Synchrotron of the Institute for Nuclear Study (INS), University of Tokyo. The converter was a 0.05-mm-thick Pt plate. The target consisted of CsCl disks of 1–4 g/cm^2 in thickness and 2.5 cm in diameter stacked with Al beam monitors of 270 mg/cm^2. The beam intensity, which was 10^7 to 10^9 equivalent quanta per second, was monitored with a Wilson-type thick chamber quantameter at INS, though the photon intensity used in the yield calculation for $E_0 \geq 100$ MeV was obtained from the monitor reaction ^{27}Al$(\gamma,2pn)^{24}$Na (Ref. 21). The photon intensity for $E_0 = 30$–65 MeV was obtained from ^{197}Au$(\gamma,n)^{196}$Au (Refs. 22 and 23) in gold monitor foils. The average beam intensity from the LNS and ETL Linacs was 10^{12}–10^{13} equivalent quanta per second.

After irradiation, barium isotopes were separated with barium carrier and purified from an aqueous solution of the CsCl target by a carbonate, nitrate, and carbonate precipitation cycle, and finally obtained as a $BaCO_3$ precipitate on a millipore Teflon filter. Xenon was adsorbed onto cooled charcoal after digesting from a melted CsCl disk and sealed in a glass ampoule. The gamma-ray measurements were performed with high-purity Ge detectors of 1.6–1.7-keV resolution at 1332 keV coupled each with a 4K pulse-height analyser. The characteristic photopeaks were evaluated with an automatic peak-search program of Komura.[24] Peak assignments were based on the energy and half-life, and the detector efficiency was determined with calibrated ^{152}Eu and uncalibrated ^{182}Ta sources of the same size as the sample. The relevant nuclear data were taken from recent compilations,[25,26] and are shown in Table I. The chemical yields were determined by the weight of $BaCO_3$ as well as by a comparison of the photopeak counts of 496 keV of ^{131g}Ba, 81 keV of ^{133g}Xe, 233 keV of ^{133m}Xe, and/or 148.9 keV of ^{123}Xe with those from a untreated CsCl disk from the same irradation.

III. RESULTS AND DISCUSSIONS

The measured yields in units of μb per equivalent quanta (μb/eq.q.) are given in Table II. The results obtained from replicate measurements are listed in separate entries. The associated errors are one standard deviation due to counting statistics. The yields of ^{133m}Xe and ^{133g}Xe were measured for $E_0 = 300$ (only for ^{133g}Xe), 500, 700, 800, 900, and 1000 MeV, but the quality of the data was poor because of low beam intensities of 10^7 eq.q. per second and of low photopeak counts used in the chemical yield evaluation. The yield measurements of ^{133m}Ba, $^{131m,m+g}$Ba, $^{129m,m+g}$Ba (and ^{129}Cs as the ^{129}Ba daughter), ^{128}Ba, ^{127}Ba, ^{126}Ba, and ^{124}Ba were more extensive, i.e., for $E_0 = 30$ to 1050 MeV in steps of 50 MeV or less. Only the upper limits were obtained for the Ba yields at low E_0.

A. Yield curves

Variations of the Xe and Ba yields with E_0 are illustrated in Figs. 1(a)–1(j). The insets in Fig. 1(a)–1(i) show details in the threshold region for pion production. Arrows on the E_0 axis indicate the Q values for the produc-

TABLE I. Relevant nuclear data for yield measurements.

Nuclide	Half-life	γ-ray energy measured (keV)	Fractional abundance (%)
^{133m}Ba	38.9 h	276.1	17.5
^{131m}Ba	14.6 min	108.5	55.2
^{131}Ba	11.8 d	496.3	47.1
^{129m}Ba	2.13 h	182.3	47.0
^{129}Ba	2.20 h	411.5	22.7
^{128}Ba	2.43 d	273.4	14.5
^{127}Ba	12.7 min	114.8	9.26
^{126}Ba	1.67 h	233.6	20.4
^{124}Ba	11.9 min	169.5	21
^{129}Cs	32.1 h	371.9	31.1
^{133m}Xe	2.19 d	233.0	9.95
^{133}Xe	5.29 d	81.0	35.9
^{123}Xe	2.08 h	148.9	48.6
^{24}Na	15.02 h	1368.5	100
^{196}Au	6.18 d	355.7	86.9

TABLE II. Measured yields of Ba isotopes from ^{133}Cs in unit of μb per equivalent quanta (μb/eq.q.)

E_0 (MeV)	^{133m}Ba	^{131m}Ba	^{131}Ba	^{129m}Ba	^{129}Ba	^{128}Ba
1050	65.7±6.4	162±14	336±34	168±15	387±36	306±28
	74.1±10.5	179±55	394±49	198±25	366±51	314±41
1000	58 ±5.8	204±12	251±37	143±10	311±18	232±12
	57.9±5.5	173±16	301±28	157±15	335±33	239±22
	88.3±7.3	196±11	465±28	255±15	445±46	357±29
950	80.0±10.1	290±6	336±42	215±4	400±41	300±20
900	36.2±10.3	134±11	332±7	162±8	253±41	285±33
850	63.0±5.1	220±12	385±20	199±12	437±25	295±19
800	79.2±3.3	148±14	325±14	162±6	371±16	303±13
	77.9±3.5	280±7	385±10	213±6	336±11	336±10
		198±16	454±40	281±23	513±70	391±45
750	91.1±22.5	254±35	333±42	202±28	284±44	252±46
700	74.9±9.0	109±8	245±8	139±3	180±14	219±38
	62.0±12	148±10	316±21	168±12	234±28	236±27
650	42.9±5.7	185±17	328±28	171±16	302±27	270±26
600	38.4±17.8	172±9	273±22	140±7	280±44	203±11
550	76.5±11.9	194±15	320±20	180±16	292±30	281±30
500	50.8±23.3	191±22	295±27	132±5	444±66	243±45
	72.1±6.8	216±20	295±29	153±13	318±30	253±23
	57.0±4.7	209±12	339±10	184±7	325±15	261±10
		266±30	406±51	232±28	352±43	239±49
450	59.5±8.8	206±18	371±22	175±15	367±40	290±34
400	37.6±23.0	115±48	305±46	108±9	149±62	176±11
	56.6±5.0	197±4	275±9	166±4	273±26	252±11
350	34.2±8.8	146±5	241±14	123±4	282±24	162±27
330		191±13	321±41	160±15	209±45	
305	40.3±2.4	88.5±2.8	173±5	80.2±2.4	137±6	107±4
	38.2±3.2		157±5	98.3±2.8	112±8	94.0±7.7
	49.2±1.8	113±7	203±4	94.2±2.0	160±7	123±5
	39.0±1.4		158±2	74.3±1.5		94.5±3.3
300	43.2±4.9	134±4	235±12	119±4	199±16	168±11
250	41.4±2.0	65.3±1.8	154±4	46.3±1.2	96.4±7.8	54.6±2.2
	47.4±3.4	81.3±29.0	166±10	50.8±3.3		62.5±4.1
230	25.9±1.9	60.5±4.1	93.2±6.6	21.1±1.4	38.1±2.8	16.9±1.3
220	25.0±2.0	46.7±1.8	86.8±3.2	19.3±0.7		16.2±1.2
	23.3±0.3	48.0±0.6	80.5±1.4	12.9±0.2	22.0±0.3	8.05±0.25

Table II. (*Continued*).

E_0 (MeV)	^{133m}Ba	^{131m}Ba	^{131}Ba	^{129m}Ba	^{129}Ba	^{128}Ba
210	26.4±1.6	47.8±2.7	81.0±4.6	11.3±0.6	20.3±1.1	5.05±0.55
195	17.2±0.6	27.4±0.8	54.1±1.6	3.40±0.11	5.34±0.26	1.83±0.26
175	10.3±0.2	12.9±0.3	17.4±0.8	1.83±0.03	3.13±0.23	1.39±0.08
160	8.01±0.65	7.27±0.49	12.1±0.7	1.53±0.08		0.95±0.17
150	3.59±0.41	5.22±0.68	7.56±0.87	0.79±0.09	1.30±0.15	0.52±0.06
149	3.70±0.19	5.60±0.19	9.65±0.35	1.03±0.04	1.67±0.09	0.76±0.08
140	4.23±0.13	6.66±0.17	11.2±0.5	1.19±0.03	2.08±0.07	0.68±0.04
130	3.36±1.07	4.35±1.34	7.17±2.25	0.61±0.19		
104	4.20±0.21	3.60±0.19	6.99±0.57	0.317±0.023	0.67±0.13	0±0.014
100	2.64±0.31	2.84±0.33	5.10±0.60	0.259±0.030		
65	1.57±0.03	0.66±0.01	1.16±0.02	0.0018±0.0003	0.007±0.004	0±0.011
64	1.29±0.02	0.58±0.07	0.98±0.34	0±0.0048	0±0.010	0±0.21
55	1.25±0.08	0.26±0.01	0.52±0.05	0±0.0049	0±0.052	0±0.89
45	0.69±0.07	0.058±0.005	0.076±0.010	0±0.0009	0±0.010	0±0.025
40	0.65±0.02	0.021+0.001	0.015±0.007	0±0.0039	0±0.032	0±0.054
30	0.21±0.0002	0±0.0002	0±0.04	0±0.0007	0±0.005	0±0.010

E_0 (MeV)	^{127}Ba	^{126}Ba	^{124}Ba	^{133m}Xe	^{133}Xe
1050	106±11	75.7±6.6	11.4±4.4		
	130±17	90.0±11.3	14.7±3.9		
1000	115±11	74.9±4.8			
		64.6±6.1		17.5±9.7	24.2±4.6
	146±12	120.6±7.0	14.3±1.7		
950	168±8	95.9±4.3	15.3±2.7		
900		75.6±9.3		14±10	47±43
850	136±12	85.3±5.0	12.0±3.8		
800	162±15	70.6±2.8			
	133±26	102±6		13.1±1.0	17.8±1.1
	139±12	134±13	12.5±1.6		
750	149±22	85.3±12.0	13.0±2.8		
700		61.0±3.9		11±6	39±23
		74.3±4.0			
650	112±12	77.5±7.5	11.8±4.5		
600		75.2±3.6			
550	149±16	84.2±7.3	10.7±3.5		
500	131±6	71.0±7.2		18±27	32±26
	137±33	76.1±7.2			
	174±36	79.8±2.3			
	192±22	96.4±11.2	16.7±4.5		
450	175±28	62.0±15.6			
400	124±9	59.1±5.3			
		71.2±2.1			
350	109±12	43.0±3.4	3.26±2.11		
330	100±9	41.6±4.7	4.7±3.8		
305		21.3±0.9			
		26.7±1.6			
		33.2±1.1			
		22.1±1.5			
300	62.3±5.2	31.0±2.0			10.9±1.4
250		2.62±0.12			
		3.03±0.22			
230	2.58±0.26	0.95±0.05			
220		1.31±0.08			
	1.19±0.54	0.39±0.03	0.028±0.237		

Table II. (*Continued*).

E_0 (MeV)	^{127}Ba	^{126}Ba	^{124}Ba	^{133m}Xe	^{133}Xe
210	0.91±0.23				
195	0.45±0.08	0.119±0.025			
175	0.336±0.024	0.065±0.011			
160		0±0.222			
150	0.115±0.020	0.007±0.002			
149		0.016±0.012			
140	0.110±0.013	0.019±0.009	0.007±0.160		
130		0±0.205			
104		0±0.017			
100		0±0.11			
65		0±0.020			
64		0±0.0091			
55		0±0.028			
45		0±0.014			
40		0±0.064			
30		0±0.0012			

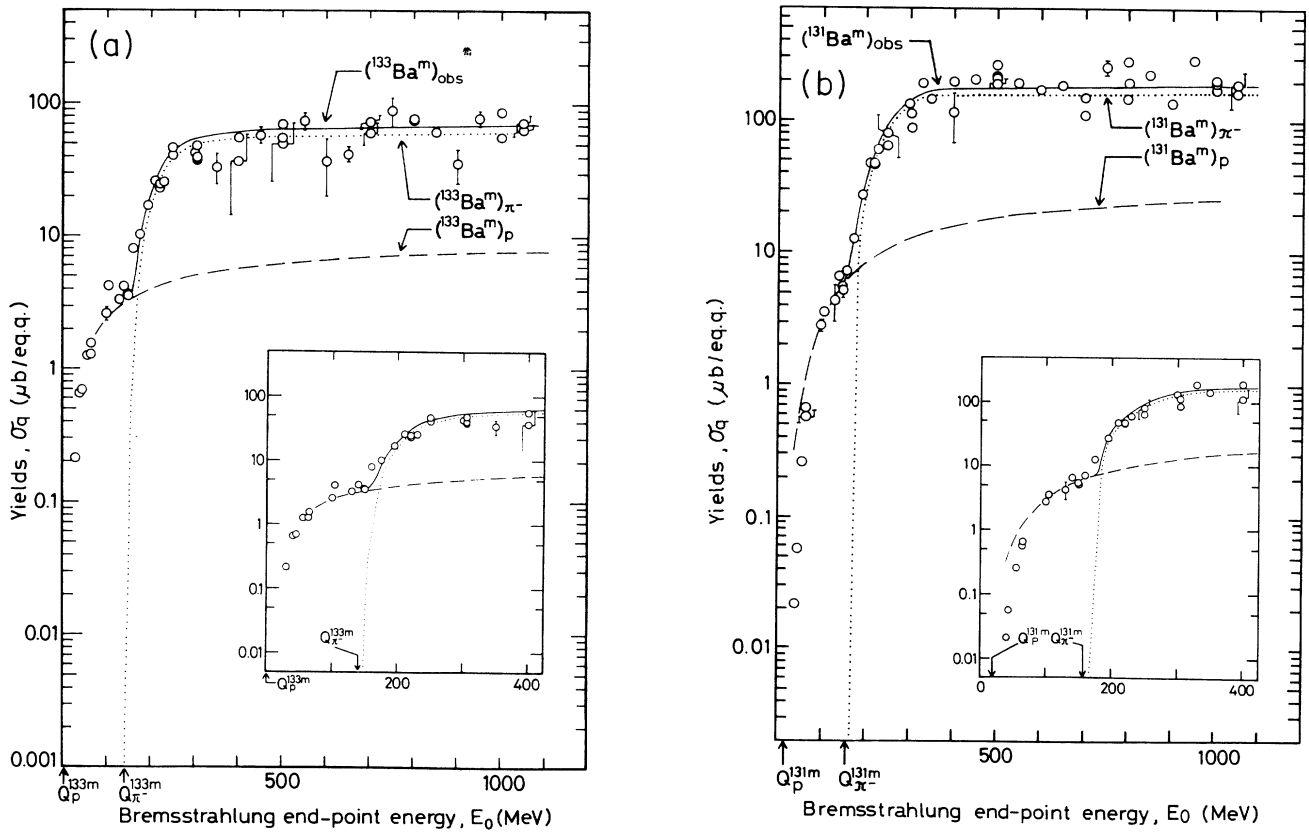

FIG. 1. The observed yields of Xe and Ba isotopes from ^{133}Cs as a function of maximum end-point energy E_0 and the component analysis. (a)–(i) The observed Ba yields shown by open circles are connected by a solid line. The inset is an expanded one in the threshold region. The dashed line indicates the yields from secondaries (see Sec. III C of the text for evaluation). The dotted line is the difference between the solid and dashed lines and regarded to be the yield from ^{133}Cs$(\gamma,\pi^- xn)^{133-x}$Ba. (j) Open circles with dotted error bars are for ^{133m}Xe and closed ones with solid bars are for ^{133g}Xe. Curves are to guide the eye. Secondary correction was not possible due to insufficient data points. Arrows on E_0 axis show the Q values for the secondary and photopion reactions. Q_n and Q_p refer to neutron and proton induced reactions, respectively.

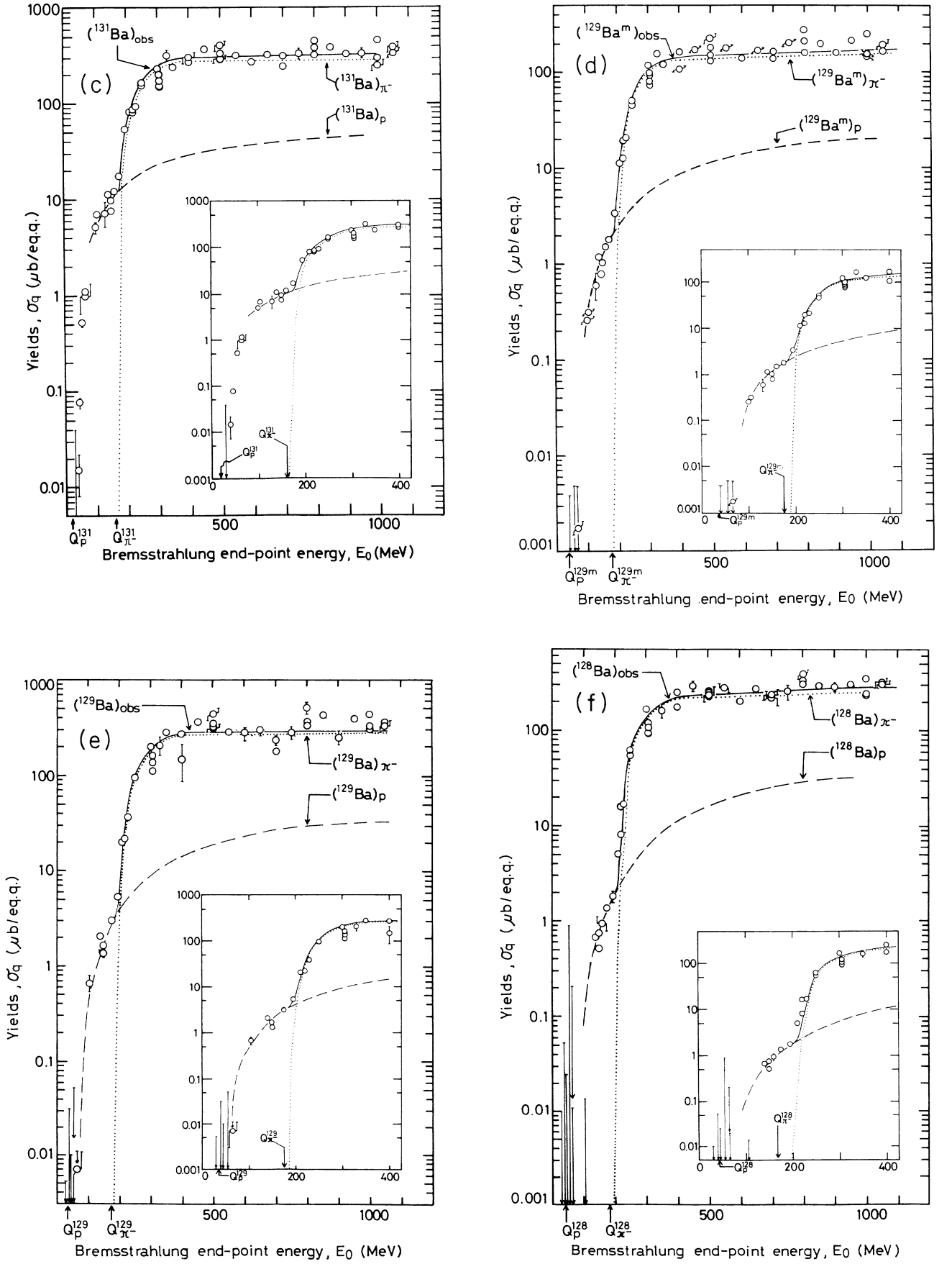

FIG. 1. (*Continued*).

tion of radionuclides, noted with their mass numbers from (n,p), $(p,x'n)$, and $(\gamma,\pi^{\pm}xn)$ reactions, i.e., Q_n^{133}, $Q_p^{134-x'}$, and $Q_{\pi^{\pm}}^{133-x}$, respectively. Error bars are based on the values given in Table II. For data points without error bars the statistical uncertainty is within the size of the symbols. There are some discrepancies among the yield values for the same or similar E_0. Discrepancies exceeding counting statistics arose mostly from our early

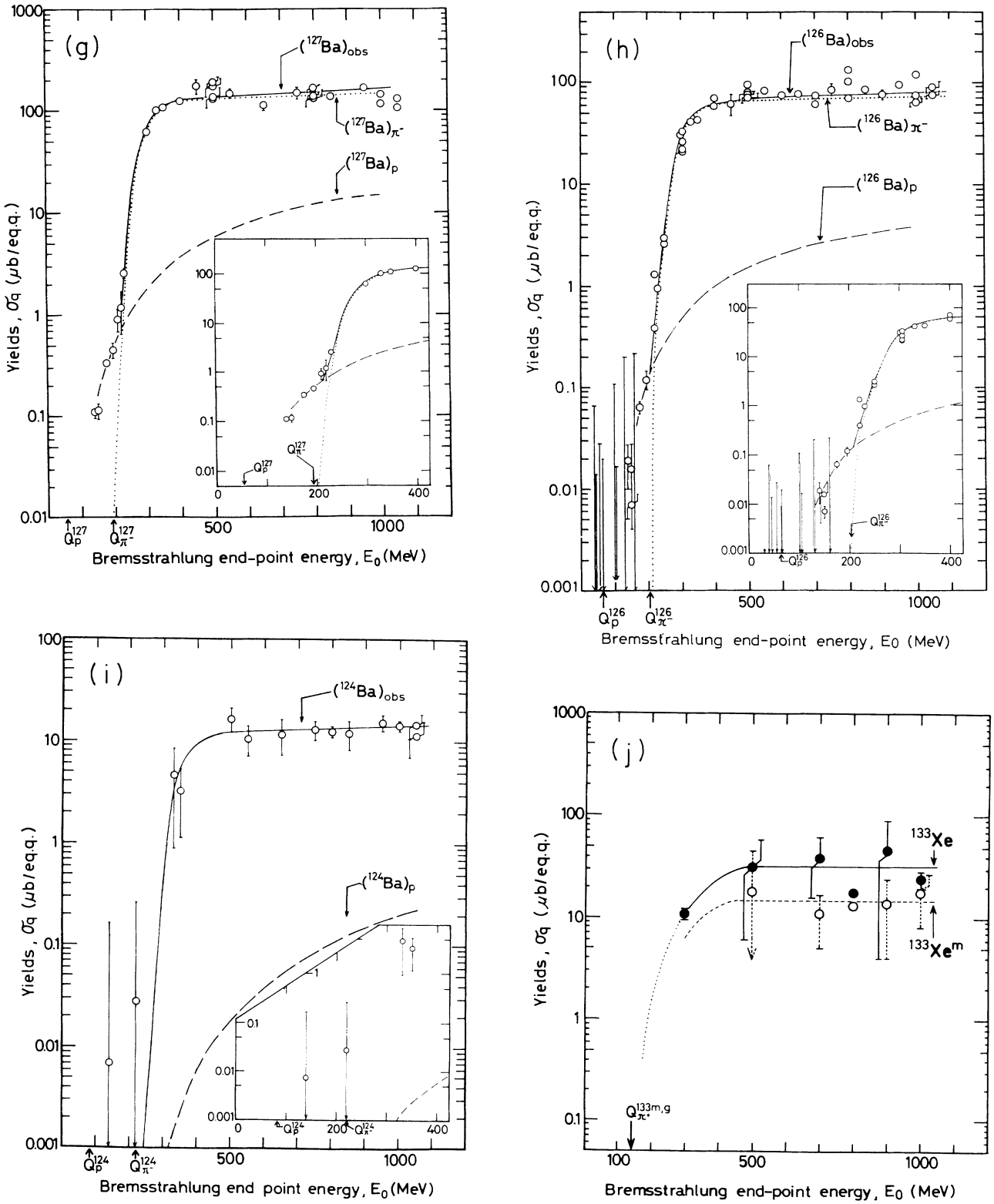

FIG. 1. (*Continued*).

measurements with insufficient beam intensities, and probably were caused by such systematic errors as large fluctuations in beam intensity. The multiple measurements resulted in the yield data converging on a smooth solid curve shown in the figures. It is noted that the yields of Ba isotopes at $E_0=30$ to 250 MeV ($\lesssim\pm1\%$) measured at the LNS linac are smoothly connected to those for $E_0=300$ to 1050 MeV ($\pm0.3\%$) measured at the INS synchrotron. The values at $E_0=305$ MeV measured at the ETL linac tend to be somewhat lower than the interpolated ones from the LNS and INS measurements. However, this discrepancy is within the range of scattering.

Appreciable yields of Ba isotopes were observed at E_0 lower by several to a few tens of MeV than Q_{π^-}, and the reaction thresholds are consistently higher than Q_p. After a steep rise from the threshold, the yields attain a plateau, or a shoulder, which emerges around $E_0=100-200$ MeV, and again increase rapidly to attain a second plateau. The second rise starts from E_0 very close to Q_{π^-}. This feature is clear evidence for the expected existence of two components: one is ascribable to a secondary proton-induced reaction of $^{133}\mathrm{Cs}(p,x'n)^{134-x'}\mathrm{Ba}$ and the other is to $^{133}\mathrm{Cs}(\gamma,\pi^-xn)^{133-x}\mathrm{Ba}$ reaction. The former is superposed on the latter at $E_0\gtrsim Q_{\pi^-}$. The decomposition of the observed yields into two components [the dashed and dotted curves in Figs. 1(a)–1(i)] is described in Sec. III C.

The observed thresholds $(E_p)_{\mathrm{th}}$ in E_0 of the secondary reactions, $^{133}\mathrm{Cs}(p,x'n)^{134-x'}\mathrm{Ba}$, are progressively higher for larger x' than Q_p. Recalling that E_0 is the bremsstrahlung maximum end-point energy and $(E_p)_{\mathrm{th}}$ the observed threshold energies in E_0 of the secondary-proton–induced reactions through $(\gamma,xnyp)$ reactions in the target by the same bremsstrahlung, the relationship of $(E_p)_{\mathrm{th}}$ and Q_p reflects the energy spectra of protons produced in the CsCl target. Actually, $(E_p)_{\mathrm{th}}$ was found to vary linearly with Q_p.

The variation of the yields after the second steep rise is not appreciable within the experimental uncertainty for all radionuclides observed, and suggests that the photons responsible for the production of these nuclides are mostly of energies lower than 400 MeV, but higher than 140 MeV (pion threshold), in accordance with the reported yield curves for $(\gamma,\pi^\pm)$ reactions on complex nuclei[5–9] and for (γ,π^-xn) reactions on ^{51}V (Refs. 5, 7, 9–13). See Sec. III C for further characteristic features of the (γ,π^-xn) yields.

B. Depth profiles

Additional measurements of the Ba yields were performed on an excessively thick target stacked with many disks of CsCl and foils of Al and Ni at $E_0=500$, 700, and 800 MeV in order to investigate the effects of target thickness to the radioactivity yields. Targets (and radiator) have to be thin enough to avoid effects of attenuation and build-up of photons and secondary particles produced in the targets, but to be thick enough to obtain good statistics. The results of the depth profiles were essentially the same for the three E_0. The 800-MeV result is shown in Fig. 2, where radioactivities per unit weight of the targets are normalized to those of the front target. The numbers in parentheses are the Q values in MeV for the production of isotopes of Ni, Co, V, and Mn from ^{58}Ni, ^{24}Na from ^{27}Al, and Ba from ^{133}Cs. The two values for ^{131}Ba and ^{126}Ba are shown: the one on the left is for $^{133}\mathrm{Cs}(p,x'n)$ and the other on the right is for the $^{133}\mathrm{Cs}(\gamma,\pi^-xn)$ reaction.

The yields of the Ba isotopes, together with ^{48}V, ^{54}Mn, and ^{24}Na, all from reactions with Q values larger than about 25 MeV, do not increase in the target depth, contrary to the expected trend for secondary particle effects. The degree of the decrease with depth is qualitatively in the order of the increase of the particle multiplicity or of the Q value, if Ba production is assumed to be from the (γ,π^-xn) reaction. The yields of ^{57}Ni expected from $^{58}\mathrm{Ni}(\gamma,n)$ and $(n,2n)$, the Q value of which is 12 MeV, increase rapidly with depth, while those of ^{56}Ni from $^{58}\mathrm{Ni}(\gamma,2n)$ and $(n,3n)$ of $Q=23$ MeV, and ^{58}Co from $^{60}\mathrm{Ni}(\gamma,pn)$ and $^{58}\mathrm{Ni}(n,p)$ of $Q=20$ MeV, increase slightly with depth. Productions of ^{57}Ni and ^{56}Ni from ^{60}Ni (26.10%) and the other heavier Ni isotopes would be less important than those from ^{58}Ni (67.76%). The decrease and/or increase of the yields may be explained as being caused by absorption of the bremsstrahlung, mainly due to e^+e^- pair creation and a build up of secondary low-energy photons and particles in the target stack. This results at depth in the suppression by the absorption of photons of energies above the pion threshold and in enhancement of, in addition to absorption of the photons responsible for the reactions of smaller Q values.

From the profile, a target stack including monitor foils of thickness less than 4 g/cm^2 was concluded to give no significant difference in the yield, and the yields presented in Table II and Fig. 1 are those obtained from CsCl targets of such limited thickness. It is also concluded from the above observation that the secondary contribution can hardly be estimated quantitatively from the depth

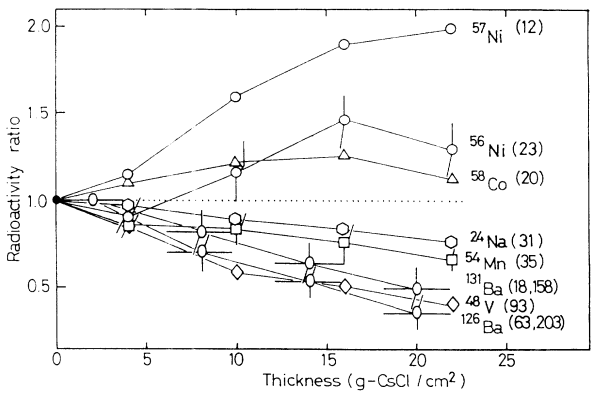

FIG. 2. Depth profiles of yields in a thick target. A stack of CsCl disks with Al and Ni foils inbetween was irradiated with bremsstrahlung of $E_0=800$ MeV, and the radioactivities per unit weight were normalized to those of the front target. Numbers in parentheses are the Q values in MeV for production of indicated nuclides. The two entries in the parentheses for ^{131}Ba and ^{126}Ba are the Q values of $^{133}\mathrm{Cs}(p,x'n)$ reactions (left) and of $^{133}\mathrm{Cs}(\gamma,\pi^-xn)$ reactions (right).

profile, in contrast to the case of charged-particle irradiation.

C. Correction for secondary reactions

The contribution of secondary reactions to the observed Ba yields was then estimated from the shoulder at $E_0 < Q_\pi$ in the yield curve. The estimation at $E_0 > Q_\pi$ was performed on the basis of the reported photoproton spectra at 40° (Ref. 27) and 72° (Ref. 28) from ^{12}C and some other complex nuclei[29] and the measured and calculated excitation functions for $^{133}Cs(p,x'n)^{134-x'}Ba$ (Ref. 30). Calculation of the proton excitation functions was carried out with the ALICE code.[31,32] For $E_p \geq 90$ MeV, the proton cross sections were assumed to decrease exponentially, i.e., $\sigma(90\ \text{MeV})\exp(-aE_p)$, a being a parameter obtained by fitting to the ALICE results at $E_p \leq 90$ MeV. The photoproton spectra at higher energies were assumed to be isotropic for the heavier target under study and originated from a quasideuteron mechanism with the Levinger constant, $L = 5-13$ (Ref. 27). The photoproton spectra at low energies were not available; they were assumed to be Maxwellian. The absolute values were estimated by fitting the calculated ^{131}Ba yields and $^{51,49}Cr$ yields from the $^{51}V(p,x'n)$ reaction[9] to the corresponding ones observed below Q_{π^-}, assuming that the latter yields are entirely from the secondaries. A good fit to the yields of ^{131}Ba was obtained, and is shown by the dashed curve denoted $(^{131}Ba)_p$ in Fig. 1(c). The $(Ba)_p$ yields for the other Ba nuclides calculated with the same proton spectrum were adjusted by multiplying them by factors of 1.8 for ^{129}Ba, 1.4 for ^{128}Ba, 2.0 for ^{127}Ba and 2.0 for ^{126}Ba, keeping the shapes as calculated, to obtain good fits to the observed shoulders. For the metastable isomer yields, the ALICE results for the formation cross sections of the ground-state isomers were tentatively used and good fits to the observed yields of $(^{133m,131m,129m}Ba)_p$ at $E_0 \lesssim Q_{\pi^-}$ were obtained by multiplying the calculated results by 0.12, 0.49, and 1.14, respectively. The different adjustments of the calculated $(^{134-x'}Ba)_p$ required in the fitting suggest that ambiguities still remain in the photoproton spectra used in the calculation. The results of the fitting are shown by the dashed curves, and the subtraction of the $(^{134-x'}Ba)_p$ from the observed yields results in the net yields which are shown by the dotted curves noted as $(^{133-x}Ba)_{\pi^-}$ in Fig. 1(a)–1(i). The relative contribution of the secondaries, $(^{134-x'}Ba)_p$, to the observed yields, $(^{133-x}Ba)_{obs}$, at $E_0 \geq 500$ MeV decreases with increase of x'. At $E_0 = 1000$ MeV they are about 15% for $^{133m}Ba(x'=1)$, 14% for $^{131m,m+g}Ba(x'=3)$, 10% for $^{129m,m+g}Ba(x'=5)$, 7% for $^{128}Ba(x'=6)$, 6% for $^{127}Ba(x'=7)$ and 5% for $^{126}Ba(x'=8)$. The amount of ^{124}Ba from $^{133}Cs(p,9n)$ was estimated from this trend, but we were unable to obtain $(^{133}Xe)_n$ from $^{133}Cs(n,p)$ due to a lack of $(^{133}Xe)_{obs}$ at $E_0 \lesssim Q_{\pi^+}$. The yields of ^{133}Xe and ^{133m}Xe are regarded to be the upper limits of the $^{133}Cs(\gamma,\pi^+)$ yields.

D. Mass yield curves

Mass yield features are shown in Fig. 3. Here, the yields of the $^{133-x}Ba$ from $^{133}Cs(\gamma,\pi^- xn)$ reactions are plotted against the number (x) of neutrons emitted at some selected E_0, compared with those of $^{51}V(\gamma,\pi^- xn)^{51-x}Cr$ as reported in Ref. 9. For $E_0 = 400$ to 1050 Mev, the average values are taken. 1 standard deviation of the mean is shown by error bars. Also plotted by elongated diamonds are the averages of the measured yields of ^{133m}Xe and $^{133(m+g)}Xe$, not corrected for secondaries. The open symbols connected with dotted curves are for the yields of the high-spin metastable isomers (m) and the closed symbols connected with solid curves include the yields of the low-spin ground-state isomers (g). The mass yield patterns for m and $m+g$ look quite similar at each E_0. The shapes of the mass yield curves are quite different for the two targets. The yields for $^{133-x}Ba$ from ^{133}Cs peak at $x \approx 3$ for $E_0 = 250$ to 1050 MeV, and the excitation energies left in the target nucleus after π^- emission are sufficiently high to evaporate 7 to 9 neutrons with appreciable probability. It is noted for ^{133}Cs that multiple neutron emission is far more probable than the (γ,π^-) channel which has no prominent E_0 dependence. The mass yield patterns[9] for a lighter target, ^{51}V for $x = 0$, 2, and 3, show a systematic variation quite different from those of ^{133}Cs; the maximum yields occur at $x \approx 0$ in ^{51}V $(\gamma,\pi^- xn)$ reaction even for $E_0 = 400-1000$ MeV. For both targets, the (γ,π^+) channel is a factor of 5 lower than the (γ,π^-) reaction at all E_0 studied.

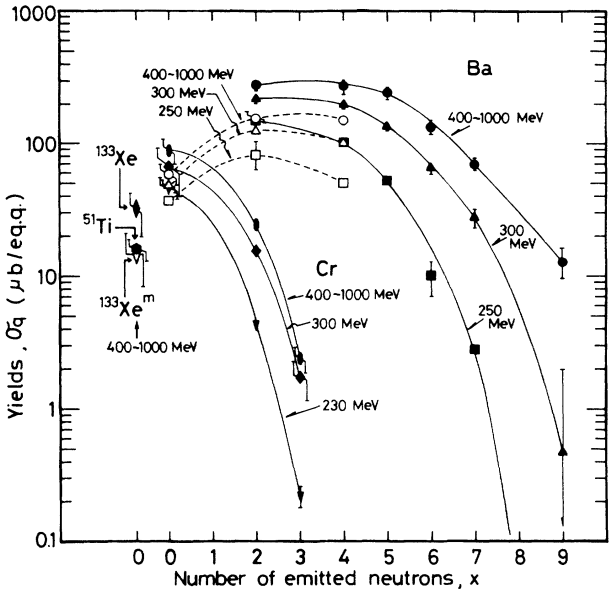

FIG. 3. Mass yield features of (γ,π^+) and $(\gamma,\pi^- xn)$ reactions on ^{133}Cs and ^{51}V targets at selected E_0. Average values are taken for $E_0 = 400$ to 1050 MeV. Closed symbols connected with solid curves are for the ground-state isomers and the open ones with dotted curves (only for ^{133}Cs target) are for the metastable isomers. The values at $x = 0$ on the left are for (γ,π^+) and at $x = 0$ on the right and $x = 1$ to 9 are for $(\gamma,\pi^- xn)$. The ^{133}Xe value is an upper limit for (γ,π^+). The data on ^{51}V are from Ref. 9.

The excitation energies left after pion emission are approximated by the sum of neutron separation energies (7 MeV/neutron on average) of the product nuclides. Aver-

aged neutron multiplicities $\bar{x}$ of 2 and 7 for the Cr and Ba yields are 14 and 50 MeV, respectively. Their ratio of 3.5 is consistent with the ratio of the target neutrons, $N_t(^{133}\text{Cs})/N_t(^{51}\text{V})=3.4$. This seems to suggest that all of the neutrons in the target nucleus are equally involved in pion (π^-) production.

E. Unfolding of yield curves

The Ba yields $\sigma_q(E_0)$, corrected for secondary reactions were unfolded into cross sections per photon of energy k, $\sigma(k)$, after the method of Tesch[33] with the aid of the LOUHI-82 code.[34] In the unfolding calculation the yield values of $\sigma_q(E_0)$ were based on the smoothed median curves shown by the dotted curves in Fig. 1(a)–1(i); the Schiff spectrum[35] was used to approximate the bremsstrahlung production cross section. The results for $\sigma(k)$ are illustrated in Fig. 4: (a) is for the isomer pairs and (b) is for the ground states, respectively. The uncertainty in $\sigma(k)$ was estimated to be about (30–50)% at peak at most from the range of scattering of the observed yields and from ambiguity inherited from unfolding process.

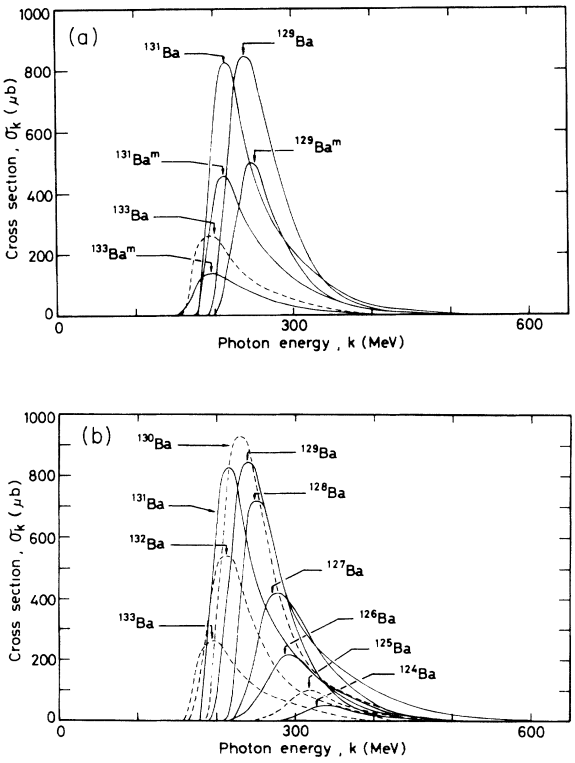

FIG. 4. Cross sections $\sigma(k)$, in unit of μb per photon, as a function of photon energy k, obtained by unfolding of the yield curves of Fig. 1. (a) shows the isomeric pairs and (b) shows the ground state isomers. The dashed curves show $\sigma(k)$ for ^{133g,132,130,125}Ba as estimated by interpolation of peak energies, FWHM and FWTM of the cross-section curves. The unfolding was based on the Schiff spectrum for bremsstrahlung and the smoothed yield curves (dotted curves) in Fig. 1. Uncertainty in magnitude is estimated to be about (30–50)% from the range of scattering of the observed data and that in peak energy less than about 10 MeV. Ambiguity inherited from unfolding process was taken into consideration in the estimation.

The shape of peak cross sections as a function of neutron multiplicity x is quite the same as the mass yield curve of 400 to 1000 MeV in Fig. 3. The peak energy was found to increase from 210 to 340 MeV with increase of $x=0$ to 9, as shown together with those of $^{51}\text{V}(\gamma,\pi^- xn)$ reaction in Fig. 5. The uncertainties in the individual peak energies were estimated also from those originating in the range of data scattering and unfolding, and an average size of the uncertainty was obtained to be less than 10 MeV from those including other targets (Ref. 36). All the excitation curves obtained here are of similar resonant shape with FWHM of 70±15 MeV, full width at quarter maximum (FWQM) of 45±10 MeV and full width at tenth maximum (FWTM) of 180±25 MeV. The widths increase slightly, though within the ranges of uncertainty, with increase of x from 0 to 9. Unmeasured cross sections for $x=1$ (^{132}Ba), $x=3$ (^{130}Ba), and $x=8$ (^{125}Ba) were then estimated by interpolation of peak energies and peak cross. FWHM, FWQM, and FWTM were taken to be 70, 45, and 180 MeV, respectively. A linear relationship of thresholds and Q values was assumed. The estimated cross sections are shown as dashed curves in Fig. 4.

It has been reported that nonresonant absorption of photons due to Born terms is dominated at thresholds of single pion photoproduction of proton and neutron, the cross sections of which increase steeply above 140 MeV (Ref. 3). The threshold of Δ resonance is then displaced to higher energy by about 30 MeV, followed by a gentle increase of the cross sections to a magnitude at a peak of one-half to two-thirds of that due to the nonresonant process, which results in the total $\sigma(k)$ for the $(\gamma,\pi^{\pm})$ excitation curve with a bump at around 210 MeV (Ref. 4). It is, however, difficult to distinguish these nonresonant and

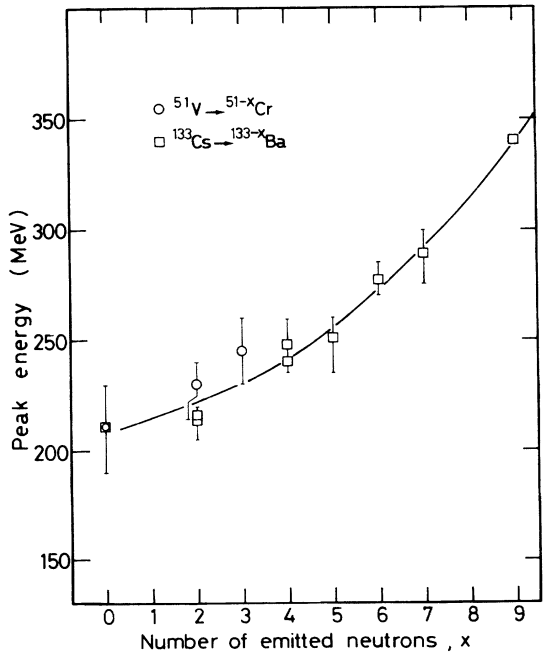

FIG. 5. Variation of peak energies of the excitation curves for the photopion reactions on ^{133}Cs and ^{51}V as a function of neutron multiplicity x.

resonant contributions from the present results because of no significant difference in the shape of the $(\gamma,\pi^- xn)$ curves of different x beyond the quoted uncertainty. Also, one sees no sign of the bump even in the observed yield curves in Fig. 1 but in that due to the background from the secondary reactions discussed in Secs. III A and III C.

As mentioned earlier, a Monte Carlo intranuclear cascade-evaporation analysis code (PICA) developed by Gabriel and Alsmiller,[17,18] has not been well tested for $\sigma(k)$ for the production of residual nuclei from the (3,3) resonance. Our recent work[9] showed that this calculation code could reproduce our $\sigma(k)$ of $^{51}V(\gamma,\pi^- xn)^{51-x}Cr$ for $x=0$, 1, 2, and 3 and $^{51}V(\gamma,\pi^+)^{51}Ti$ within a factor of 2, provided that all the calculated results were shifted higher on the k axis by 30 MeV for ^{51-x}Cr and by 60 MeV for ^{51}Ti. The same calculation was carried out in the present work for the $^{133}Cs(\gamma,\pi^- xn)^{133-x}Ba$ reaction of much higher neutron multiplicity (x up to 9) for $k=150$ to 400 MeV. The same parameter values were chosen as those of the original authors, except for some alternative sets of cutoff energies for emitted particles. The results of the calculation with the cutoff energies of 5 MeV (one-half of the Coulomb barrier) for charged particles and 1 MeV for neutrons are plotted in Fig. 6(a)–6(d) for the odd-mass products and in Fig. 6(e)–6(h) for the even-mass products, as connected by the dotted curves to guide the eye. Events for ^{124}Ba production were too infrequent to appear in the particle histories of $(0.2-1)\times10^6$. The error bars assocated with the calculated points are statistical. The solid curves are the same as in Fig. 4. Note that the k axis is different for the two; i.e., all the peak locations of the calculated curves can be fitted very well to the experimental ones by shifting the former higher by 30 MeV, as was necessary in the case of $^{51}V(\gamma,\pi^- xn)^{51-x}Cr$. Reproduction of the peak cross sections of the even-mass products is excellent; however, for the odd-mass products the calculated peak cross sections are lower by 100% for ^{133}Ba, 15% for ^{131}Ba and 7% or less for ^{129}Ba, but higher by 50% for ^{127}Ba than the corresponding experimental ones. These features of the peak cross sections are caused by a strong even-odd effect in the calculation as depicted in Fig. 7. The even-odd feature of the PICA results for $^{51}V(\gamma,\pi^- xn)^{51-x}Cr$ was also evident. Different sets of cutoff energies for charged particles and neutrons of 10 and 0 MeV, 10 and 5 MeV, and 5 and 0 MeV, respectively, yielded still higher peak values at $x>3$ (^{130}Ba–^{127}Ba), while those at $x\leq2$ (^{133}Ba–^{131}Ba) remained the same. It is noted that in the calculation for $\sigma(k)$ for the $^{51}V(\gamma,\pi^- xn)$ reaction no prominent difference was obtained from different sets of the cutoff energies. The calculation for the high-energy part of the tail gave the $\sigma(k)$ values somewhat higher than the experimental one, though within the uncertainty of the latter. However, it may be concluded that the PICA code reproduces well the gross features of $\sigma(k)$ at the Δ resonance if the energy shift of 30 MeV for the $(\gamma,\pi^- xn)$ reaction [and 60 MeV for the (γ,π^+) reaction] is taken into account.

In Fig. 8 the sum of $\sigma(k)$ for the $^{133}Cs(\gamma,\pi^- xn)$ reaction is shown by adding all the values for $x=0$ to 9 at $k=$threshold to 500 MeV, and compared with three types of total photoabsorption cross sections. The largest contribution to the sum is from the reactions for $x=2-5$, including the estimated one for $^{133}Cs(\gamma,\pi^- 3n)^{130}Ba$, as suggested from the mass yield curves shown in Fig. 3. The peak energy of the sum is 240 MeV and its FWHM is 90 MeV. The peak energies of the sum and the individual channels are far smaller than those expected from (3,3) resonance in pion photoproduction from a free nucleon (N). The total photoabsorption cross section $\sigma_{\rm tot}$ may be regarded as a measure of the sum of the decay channels, such as $(\gamma,\pi^- xn)$, $(\gamma,\pi^{\pm,0}xnyp)$, and $(\gamma,xnyp)$. If $\sigma_{\rm tot}$ for a target of mass number A_t is taken simply to be $A_t\sigma_{\gamma N}$, $\sigma_{\gamma N}$ being an average of the single nucleon total absorption cross section,[37] $\sigma_{\gamma N}=(\sigma_{\gamma p}+\sigma_{\gamma n})/2$, as an approximation, the sum of $^{133}Cs(\gamma,\pi^- xn)^{133-x}Ba$ is shown to be only 4% of $133\sigma_{\gamma N}$ (Fig. 8). It may be noteworthy that the present sum for $(\gamma,\pi^- xn)$ would be (1.9 ± 0.6)% of the total hadronic cross section, $133\sigma_{\gamma h}$, which was obtained by Bonn, Mainz, and Saclay groups and compiled by Ahrens and O'Connell[38] and Arends.[39] This may be more reasonably accounted for by comparing the total Ba yield of 1.6 mb/eq.q. with our preliminary photspallation yields of about 105 mb/eq.q. from ^{133}Cs (Ref. 40). The difference of $\sigma_{\gamma N}$ and $\sigma_{\gamma h}$ suggests that photon is absorbed by a dynamical assembly consisting of 133 nucleons. The total inelastic cross section (dashed curve) obtained from the PICA code agrees in peak energy with both $\sigma_{\gamma N}$ and $\sigma_{\gamma h}$, if the PICA result (solid curve) is shifted by 30 MeV as noted above in the comparison of the individual $\sigma(k)$ for the $(\gamma,\pi^- xn)$ reaction. The peak cross section and the width of the PICA result are still somewhat different from $\sigma_{\gamma h}\times133$.

It is now clear in Fig. 8 that the decay channel for $(\gamma,\pi^- xn)$ is actually the simplest part of the (3,3) resonance absorption among others, being opened at the lowest excitation of the resonance absorption. The remaining channels end up in spallation with and without pion emission. The PICA calculation indicates that the $(\gamma,xnyp)$, $(\gamma,\pi^0 xnyp)$, $(\gamma,\pi^- xnyp)$, and $(\gamma,\pi^+ xnyp)$ channels with $x,y\geq0$ account for about 60%, 20%, 13%, and 7%, respectively of the total cross sections at $k=200$ to 400 MeV. Also, it is indicated in PICA that the distribution of the points (R), where the emitting particles experience the last collision in the nucleus of radius (R_0), is somewhat different for different particles and energies, but extends over a range of $R/R_0=0.1-1.0$. Most of energetic (100–200 MeV) particles come out from $R/R_0=0.4$ to 1.0 with a maximum at around $R/R_0=0.7-0.8$ for pions and 0.4–0.8 for nucleons. This may, however, be understood to be a consequence of the assumed density distribution, i.e., $\rho(R)=\alpha_i\rho(0)$, $i=1$, 2, and 3, where $\alpha_1=0.9$, $\alpha_2=0.2$, and $\alpha_3=0.01$. These results are identical with our similar comparison for $^{51}V(\gamma,\pi^- xn)^{51-x}Cr$.[9] In the case of ^{51}V, the total cross sections for the $(\gamma,\pi^- xn)$ reaction peak at 225 MeV with a FWHM of 90 MeV, and amount only to (0.6 ± 0.2)% of the $51\sigma_{\gamma h}$. Theoretical calculations based on the valence nucleon model and/or DWIA (distorted-wave impulse approximation) and PICA by the Lund

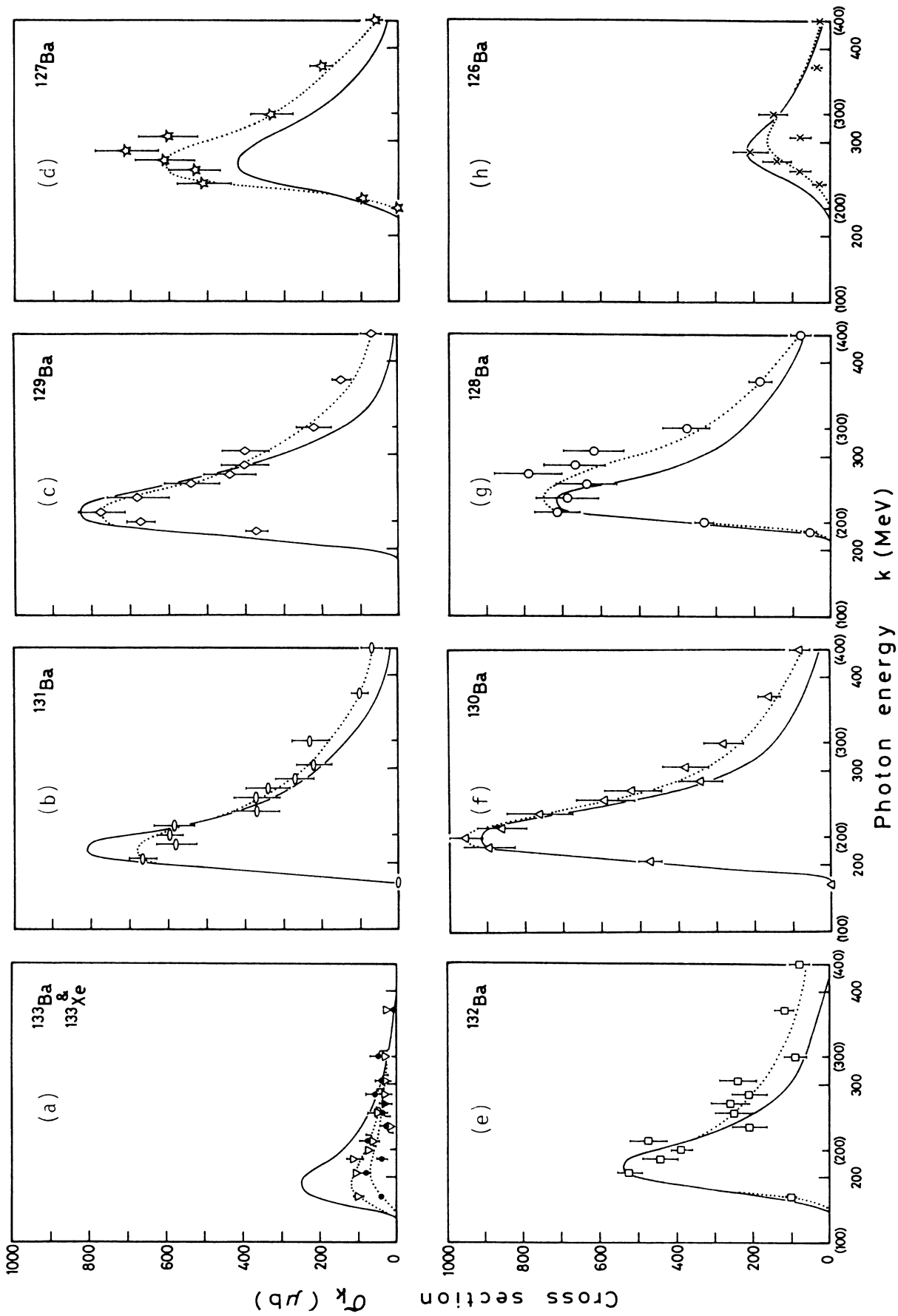

FIG. 6. Comparison of the calculated $\sigma(k)$ by PICA code (symbols with statistical errors; dotted curves to guide the eye) with the experimental ones (solid curves). (a)–(d) show odd-mass products: ^{133}Xe (closed circle), ^{133}Ba (reversed triangle), ^{131}Ba (oval), ^{129}Ba (diamond), and ^{127}Ba (star). (e)–(h) show even-mass products: ^{132}Ba (square), ^{130}Ba (triangle), ^{128}Ba (circle), and ^{126}Ba (cross). The calculation resulted in only a single value 30 ± 17 mb at 300 MeV for ^{124}Ba in the particle history of $(0.2-1)\times10^6$, and is not shown in the figure. The photon energy scale for the PICA results is shown in parentheses and the scale for the experimental results without parentheses.

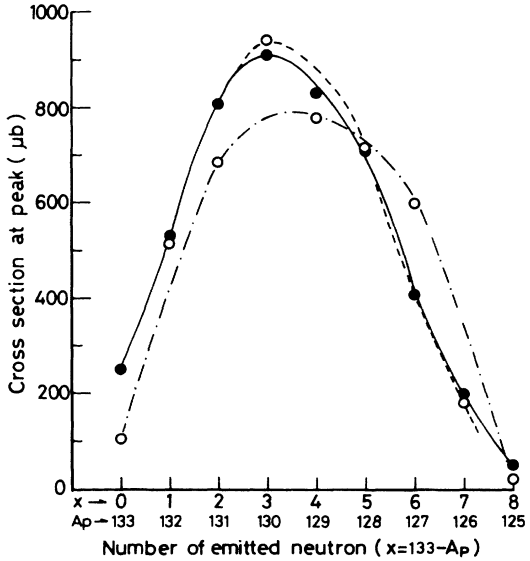

FIG. 7. Peak cross sections as a function of neutron multiplicity x for $^{133}Cs(\gamma,\pi^- xn)^{133-x}Ba$, as taken from Fig. 6. The PICA code results in an odd-even effect as shown by a dashed curve for the even-mass products (x =odd) and a dash-dotted curve for the odd-mass products (x =even). The closed circles tied by a solid curve are from the present experiment.

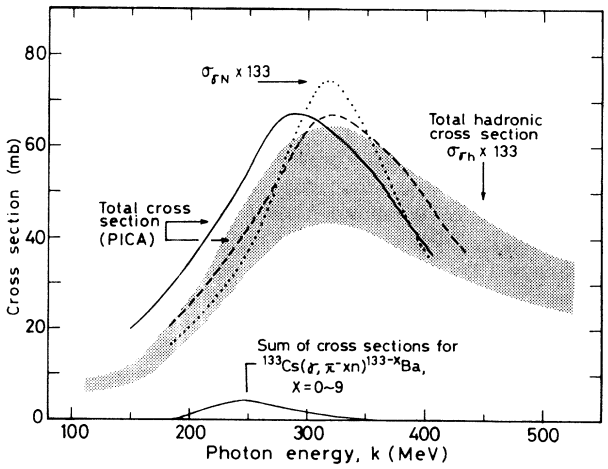

FIG. 8. Sum of $\sigma(k)$ for formation of $^{133-x}Ba$ from $^{133}Cs(\gamma,\pi^- xn)$ reaction for $x \leq 9$ and three types of the total photoabsorption cross sections. The total photoabsorption cross section was first approximated simply by $A_t\sigma_{\gamma N}$, A_t(=133) being target mass and $\sigma_{\gamma N}=(\sigma_{\gamma p}+\sigma_{\gamma n})/2$ being an average of single nucleon total photoabsorption cross sections (Ref. 37) and shown by the dotted curve. The shaded area is the range of errors of the total hadronic cross sections, $\sigma_{\gamma h}$ per nucleon (Refs. 38 and 39) multiplied by 133. Total cross section from the PICA calculation is shown by a solid curve as indicated. The dashed one is the PICA result shifted by 30 MeV in energy scale (see also Fig. 6). The small solid curve is the sum of the ^{133}Cs $(\gamma,\pi^- xn)$ cross sections for x =0 to 9 of Fig. 4(b).

group[5,8] were available for ^{51}Ti and ^{49}Cr, but both the magnitude and shape of the calculated curves were in disagreement with our observations.[9]

It is concluded that the observed features suggest that the photon reaction samples the entire nuclear volume. Detailed consideration of kinematic and dynamical effects of Δ-hole propagation in the nucleus,[41] not only on charged-pion-emitting reactions but on the other channels, is required for a more quantitative discussion, along with further systematic experiments.

ACKNOWLEDGMENTS

The authors are indebted to Dr. M. Yagi and Dr. K. Masumoto of the Laboratory of Nuclear Science, Tohoku University; Dr. T. Tomimasu and Dr. Y. Kawada of the Electrotechnical Laboratory; and Dr. K. Yoshida, Dr. Miyachi, and Dr. M. Mutou of the Institute for Nuclear Study, University of Tokyo for their invaluable cooperation in accelerator operations, and to Mr. T. Fukasawa and the other students of the Radiochemistry Laboratory of Kanazawa University in radioactivity measurements. This work was supported by a Grant-in-Aid for Scientific Research (60430012 and 01470049) of the Ministry of Education, Science and Culture of Japan.

[1] *Photopion Nuclear Physics,* edited by P. Stoler (Plenum, New York, 1979).

[2] *Nuclear Physics with Electromagnetic Interactions,* edited by H. Arenhövel and D. Drechsel, Proceedings of the International Conference on Nuclear Physics with Electromagnetic Interactions, Mainz, 1979, Vol. 108 of *Lecture Notes in Physics,* (Springer-Verlag, Berlin, 1979).

[3] I. Blomqvist and J. M. Laget, Nucl. Phys. **A280**, 45 (1977).

[4] M. K. Singham and F. Tabakin, Ann. Phys. (N.Y.) **A135**, 71 (1981).

[5] G. Nydahl and B. Forkman, Nucl. Phys. **B7**, 97 (1968).

[6] I. Blomqvist, G. Nydahl, and B. Forkman, Nucl. Phys. **A162**, 193 (1971).

[7] G. Kumbartzki and U. Kim, Nucl. Phys. **A176**, 23 (1971).

[8] I. Blomqvist, P. Janecek, G. G. Jonsson, H. Dinter, K. Tesch, N. Freed, and P. Ostrander, Phys. Rev. C **15**, 988 (1977).

[9] K. Sakamoto, M. Yoshida, T. Fukasawa, Y. Hamajima, S. Shibata, and I. Fujiwara, Nucl. Phys. **A501**, 693 (1989).

[10] R. A. Meyer and J. P. Hummel, Phys. Rev. **140**, B48 (1965).

[11] B. Bülow, B. Johnsson, M. Nilsson, and B. Forkman, Z. Phys. A **278**, 89 (1976).

[12] I. Blomqvist, P. Janecek, G. G. Jonsson, R. Petersson, H. Dinter, and K. Tesch, Z. Phys. A **278**, 83 (1976).

[13] V. di Napoli, F. Salvett, M. L. Terranova, H. G. de Carvalho, J. B. Martins, and O. A. P. Tavares, J. Inorg. Nucl. Chem. **40**, 175 (1978).

[14] I. Blomqvist, B. Bülow, A. Fredrikson, B. Johnsson, K. Lindgren, M. Nilsson, R. Petersson, O. Glomset, N. Freed, and W. Rhodes, Z. Phys. A **288**, 313 (1978).

[15] B. Bülow, B. Johnsson, G. G. Jonsson, K. Lindgren, M. Nilsson, and R. Petersson, Z. Phys. A **290**, 393 (1979).

[16] P. H. Ballentine, J. K. Hersh, H. A. Medicus, S. Planeta, F.

Potentiani, and S. Rossdentscher, in *Photopion Nuclear Physics*, edited by P. Stoler (Plenum, New York, 1979), pp. 387–389.
[17]T. A. Gabriel and R. G. Alsmiller, Jr., Phys. Rev. **182**, 1035 (1969).
[18]T. A. Gabriel, M. P. Guthrie, and O. W. Hermann, Oak Ridge National Laboratory Report No. ORNL-4687 (1971).
[19]K. Sakamoto, H. Toramoto, Y. Hamajima, K. Okada, and M. Dohniwa, Radiochim. Acta **37**, 69 (1984).
[20]M. Sugawara, T. Ichinohe, S. Urasawa, M. Oyamada, T. Kubota, A. Karihara, O. Konno, Y. Shibazaki, T. Terasawa, K. Nakahara, S. Enomoto, M. Muto, K. Shoda, and Y. Torizuka, Nucl. Instrum. Methods **153**, 343 (1978).
[21]B. Jonsson, H. Harund, and B. Forkman, Z. Phys. A **273**, 97 (1975).
[22]K. Lindgren and G. G. Jonsson, Nucl. Phys. **A166**, 643 (1971).
[23]K. Osada, T. Fukasawa, K. Kobayashi, Y. Hamajima, K. Sakamoto, S. Shibata, and I. Fujiwara, Res. Rept. Lab. Nucl. Sci. Tohoku Univ. **20**, 299 (1987).
[24]K. Komura, Technical Report of the Institute for Nuclear Study, University of Tokyo, Report No. INS-TCH-9 (1974).
[25]U. Reus and W. Westmeier, At. Data Nucl. Data Tables **29**, 193 (1983).
[26]E. Browne and R. B. Firestone, *Table of Radioactive Isotopes*, edited by V. S. Shirley (Wiley, New York, 1986).
[27]G. Andersson, P. Dougan, and W. Stiefler, Z. Phys. A **272**, 263 (1975).
[28]J. L. Matthews, W. Bertozzi, S. Kowalski, C. P. Sargent, and W. Turchinetz, Nucl. Phys. **A112**, 654 (1968).
[29]P. Dougan, B. Forkman, W. Stiefler, and J. L. Matthews, Z. Phys. **269**, 105 (1974).
[30]K. Sakamoto, M. Dohniwa, and K. Okada, Int. J. Appl. Radiat. Isot. **36**, 481 (1985).
[31]M. Blann, Annu. Rev. Nucl. Sci. **25**, 123 (1975).
[32]F. Plasil, Oak Ridge National Laboratory Report No. TM-6045, 1977.
[33]K. Tesch, Nucl. Instrum. Methods **95**, 245 (1971).
[34]J. T. Routi and J. V. Sandberg, Comput. Phys. Commun. **21**, 119 (1980).
[35]L. I. Schiff, Phys. Rev. **83**, 252 (1951).
[36]K. Sakamoto, Research Reactor Institute, Kyoto University, Technical Report No. KURRI-TR-315, 1989, p. 48.
[37]Particle Data Group, Phys. Lett. **170B**, 85 (1986).
[38]J. Ahrens and J. S. O'Connell, Comments Nucl. Part. Phys. **14**, 245 (1985).
[39]J. Arends, Bonn University Report No. Bonn-IR-88-05, 1988, and references therein.
[40]K. Sakamoto, Y. Hamajima, M. Soto, Y. Kubota, M. Yoshida, T. Hashimoto, T. Fukasawa, I. Fujiwara, and S. Shibata, Res. Rep. Lab. Nucl. Sci. Tohoku Univ. **18**, 290 (1985).
[41]J. H. Koch, E. J. Moniz, and N. Ohtsuka, Ann. Phys. (N.Y.) **154**, 99 (1984).

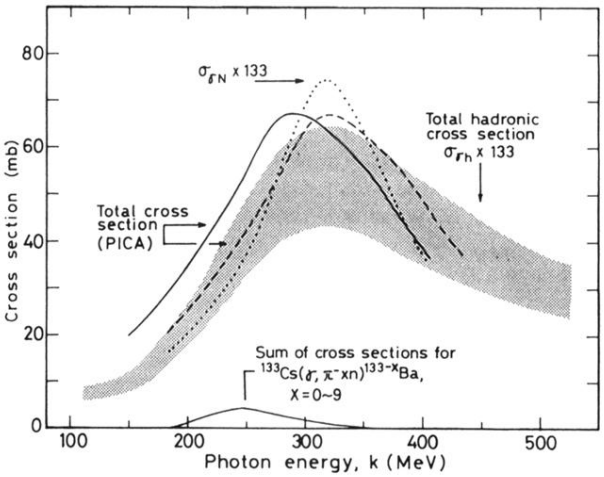

FIG. 8. Sum of $\sigma(k)$ for formation of $^{133-x}$Ba from ^{133}Cs$(\gamma,\pi^- xn)$ reaction for $x \leq 9$ and three types of the total photoabsorption cross sections. The total photoabsorption cross section was first approximated simply by $A_t\sigma_{\gamma N}$, $A_t(=133)$ being target mass and $\sigma_{\gamma N}=(\sigma_{\gamma p}+\sigma_{\gamma n})/2$ being an average of single nucleon total photoabsorption cross sections (Ref. 37) and shown by the dotted curve. The shaded area is the range of errors of the total hadronic cross sections, $\sigma_{\gamma h}$ per nucleon (Refs. 38 and 39) multiplied by 133. Total cross section from the PICA calculation is shown by a solid curve as indicated. The dashed one is the PICA result shifted by 30 MeV in energy scale (see also Fig. 6). The small solid curve is the sum of the ^{133}Cs $(\gamma,\pi^- xn)$ cross sections for $x=0$ to 9 of Fig. 4(b).